Effect of multiaxiality, stacking sequence and number of off-axis layers on the mechanical response and damage sequence of carbon/epoxy composite laminates under static loading

Kalteremidou, Kalliopi-Artemi; Hajikazemi, Mohammad; Van Paepegem, Wim; Van Hemelrijck, Danny; Pyl, Lincy

Published in:
Composites Science and Technology

DOI:
10.1016/j.compscitech.2020.108044

Publication date:
2020

Effect of multiaxiality, stacking sequence and number of off-axis layers on the mechanical response and damage sequence of carbon/epoxy composite laminates under static loading

Kalliopi-Artemi Kalteremidou[1], Mohammad Hajikazemi[2], Wim Van Paepegem[2], Danny Van Hemelrijck[1] and Lincy Pyl[1]

[1]Department of Mechanics of Materials and Constructions, Vrije Universiteit Brussel, Pleinlaan 2, 1050 Brussels, Belgium

[2]Department of Materials, Textiles and Chemical Engineering, Ghent University, Technologiepark Zwijnaarde 46, 9052 Ghent, Belgium

Corresponding author: Kalliopi-Artemi.Kalteremidou@vub.be

Abstract: The mechanical response and damage sequence of composite materials are nowadays still a topic of ongoing research. However, many parameters influencing their overall behavior are still not thoroughly taken into consideration. The effect of multiaxial stresses, the distinction between balanced and unbalanced configurations and the influence of the number of off-axis layers are just a few to mention. Experimental data regarding the effect of all these parameters on the damage progression in composites is of great importance, since it is proven that commonly used failure criteria, neglecting the occurring damage mechanisms, cannot always predict the material response. In this work, a study of the influence of all these parameters is attempted, by testing carbon/epoxy laminates with different off-axis angles to account for different multiaxiality. Both balanced and unbalanced laminates are taken into account, considering the lack of experimental evidence in literature regarding the latter case, and significant differences between the two lay-ups are reported for the first time. Finally, the influence of the number of the off-axis layers on the mechanical response in conjunction with the previous parameters is also studied through elaborate damage observations.

Keywords: A. Polymer-matrix composites (PMCs), B. Delamination, C. Damage mechanics, D. Non-destructive testing, Unbalanced laminates

1. Introduction

Composite materials are considered to be one of the most promising materials of the future for lightweight structures, owing to their great specific strength and stiffness. During the last decades, an incredible research interest has been developed in polymer composites. Scientists around the world try to develop appropriate models to predict the structural integrity of composite components for real applications [1]. For this to be achieved, the influence of multiple parameters on their mechanical response and stochastic damage behavior must be thoroughly examined.

Most of the failure criteria still being used in the theory of composite materials are based on calculation of stress states and interaction of the different stress components [2]–[5]. According to these criteria, when a specific stress state is established within a composite lamina, this layer will fail, altering the total compliance of the laminate. After recalculation of the developed stress states, the selected criteria are applied once more, and the following weaker lamina is assumed to fail when a certain stress condition is reached. However this approach, based only on calculation of stresses while neglecting the physical presence of damage, lacks in reliability since the stress state in a composite lamina can change from point to point, therefore unique values of stress components in a layer cannot be assumed [6]–[9]. Moreover, whereas the applicability of these criteria can be accepted for more common lay-ups, like for example cross-ply laminates, it is questioned when off-axis layers are inserted in the laminate [10]–[13], leading to the development of biaxial/multiaxial stress states. According to the World-Wide Failure Exercise (WWFE) [14], there is a high need for dedicated experimental campaigns focusing on the influence of multiaxial stress states on the mechanical response of composites.

Furthermore, according to the WWFE, one of the biggest weaknesses of the existing failure criteria concerns the prediction of the initial damage event during loading. While many criteria succeed in predicting the final total strength of composite laminates, there is a significant lack of reliable experimental data on the initial failure stress, the mode of damage that occurs and the practical significance of the mode of initial damage on the subsequent damage process and the post-initial

laminate performance [14]. Identifying the conditions leading to different First Ply Failure (FPF) modes and consequently to dissimilar damage processes especially under multiaxial loading is, however, of paramount importance in order to establish reliable damage-based failure criteria [15], [16]. Until now it is assumed that the damage sequence of composite materials follows a certain path, initiating in the form of fiber/matrix debondings and matrix cracks, leading afterwards to interlaminar delaminations and finally to fiber breaks [17]–[23]. However, even from the late 1990s, Varna et al. [24] mentioned the occurrence of a different damage mechanism prior to matrix cracking when certain stress conditions occur. Nevertheless, no detailed description of the conditions leading to a different damage sequence was discussed. Furthermore, detailed damage progression evidence in carbon fiber polymer laminates is much more limited in comparison to laminates with glass fibers due to the transparency of the last ones, allowing easier damage assessments. Therefore, damage studies in commonly used carbon fiber laminates are of great importance in order to enrich the existing experimental database.

Taking all above into account, this study considers the effect of different parameters on the mechanical response and damage sequence of carbon/epoxy laminates under static loading. As a first step, the influence of multiaxial stress states acting in the off-axis layers of unbalanced laminates is examined, considering the lack of experimental evidence and the limited applications making use of unbalanced lay-ups. In a previous study of the authors [25], it was proven that shear-dominated off-axis layers have a potential to lead sooner to delaminations. In this study, a stress analysis is performed, to correlate the damage sequence with the stresses in the composite laminas. In a second step, the unbalanced laminates are compared with balanced ones. Significant differences between the two cases are reported for the first time in literature to the best of the authors' knowledge. For some designs of composite laminates, the use of balanced lay-ups is often desirable in order to avoid the coupling effects between shear and extension. However, many practical applications require unbalanced or non-symmetric laminates to specifically achieve the design requirements. Characteristic examples are laminates with bending-twisting couplings for optimizing passive-adaptive flexible wing-box structures

to achieve measurable drag reduction [26], biangle laminates for improved deformations and time-dependent behavior [27], unbalanced lay-ups in morphing and bistable composites combined with piezoelectrics for energy harvesting [28], etc. Nevertheless, due to the complexities involved both in testing and modelling, there are not many works dealing with unbalanced laminates especially under multiaxial loading conditions. The current findings lead to promising conclusions regarding the potential of unbalanced lay-ups for load bearing applications. Finally, the influence of the number of the off-axis layers on the mechanical response is investigated. In order to obtain detailed damage investigations, in-situ microscopy is performed for all laminates, by attaching an optical microscope on the test bench and performing interrupted inspections while keeping the samples loaded. Moreover, to monitor damage onset, Acoustic Emission (AE) is applied, being able to indicate damage at a much earlier stress level than any optical observations [29]–[31].

2. Material selection and equipment

2.1. Description of material and testing equipment

The material used in the current study were carbon/epoxy laminates made by unidirectional fibers in the form of pre-preg plates and manufactured by Mitsubishi Chemical Corporation. The pre-pregs were cured in an autoclave for 60 minutes at a temperature of 130^{o}C and a pressure of 0.6 MPa. To follow the ASTM D3039 standard, the plates were tabbed on both sides for a length of 50 mm by using the same carbon/epoxy material in a $[45^{o}/-45^{o}]_{2s}$ lay-up. The material properties were obtained by tests on standard specimens and are presented in Table 1. Following the ASTM D3039 standard, all tested samples had a total length of 250 mm and a width of 25 mm while the thickness was equal to 1.83 mm for the considered 8-ply laminates and 2.74 mm for the 12-ply laminates which will be explained later.

The mechanical tests were performed using an MTS servo-hydraulic test bench. Uninterrupted quasi-static tests were initially performed with a constant displacement rate equal to 1 mm/min in order to obtain the mechanical properties of the laminates. Based on the findings of the uninterrupted tests,

interrupted quasi-static tests at certain load intervals were performed to investigate the damage progression of the laminates. To achieve this, a MZ125 stereomicroscope from Leica Microsystems with 8-100x magnification and 375 line-pairs/mm resolution was mounted on the test bench. The specimens were loaded until certain load levels and by keeping them tensioned, through-thickness damage observations on their free edge were performed along their gauge length. The advantage of the set-up is that load is still applied on the specimens during the observations, therefore occurring cracks are still open and visible, contradictory to the cases in which post-monitoring is performed. Prior to testing, the free edges of the samples were polished starting with SiC grit papers of 46 μm particle size and going down to 5 μm. By that, potential damage initiation positions were eliminated avoiding stress concentrations.

To obtain strain measurements, a Digital Image Correlation (DIC) VIC-3D system by Correlated Solutions was utilized. Two Charge Couple Device (CCD) cameras with 23 mm focal length lenses were used and a white/black speckle pattern was applied on the surface of the specimens. Through triangulation of the cameras and by tracking the changes of the gray value pattern in individual groups of pixels (subsets) during the deformation, strain calculations on the surface of the specimens can be obtained. A subset of 21 pixels by 21 pixels was used and a step of 7 pixels (corresponding to the distance between the center points of the adjacent subsets) was applied during the DIC analysis. The features of the DIC configuration are in detail shown in Table 2, including the obtained resolution and sensitivity of the system. At the same time, an MTS 50 mm extensometer was used to validate the longitudinal strain measurements. An AE system consisting of two sensors was also utilized in order to obtain the acoustic activity of the samples during testing. Based on the emitted acoustic signals after certain damage incidents, AE can give information on the occurring damage. A Mistras Group acquisition system was used, and the two sensors were mounted on the samples with a relative distance of 80 mm using vaseline.

In Figure 1, the experimental set-up under consideration is presented.

2.2. Rationale of lay-up selection

As mentioned earlier, the influence of three parameters is studied in this work, i.e. the occurrence of multiaxial stresses, the comparison between balanced and unbalanced lay-ups and the number of off-axis layers. For this reason, six laminates were tested under static conditions. $[0^o/\theta]_{2s}$ unbalanced laminates were initially tested for two different θ values to account for dissimilar multiaxial stresses in the off-axis layers. Results related to the damage behavior of these two laminates have already been presented in [25]. The angle values θ were chosen based on calculations from the Classical Laminate Theory (CLT). Considering that most failure criteria make use of stresses and strains in the material coordinate system, it was decided to choose the angle of the off-axis layers based on the biaxiality ratios λ, which express the relation between the normal and shear stresses in the principal directions. Specifically, the λ_1, λ_2 and λ_{12} ratios were used, defined as:

$$|\lambda_1| = \left|\frac{\sigma_2}{\sigma_1}\right|, |\lambda_2| = \left|\frac{\tau_{12}}{\sigma_1}\right|, |\lambda_{12}| = \left|\frac{\tau_{12}}{\sigma_2}\right| \quad (1)$$

where σ_1 and σ_2 are the in-plane longitudinal and transverse stress components and τ_{12} is the in-plane shear stress in the material coordinate system [32]. Special focus was given to the λ_{12} ratio, linking the in-plane transverse with the shear stress, to examine the influence of their combination on the mechanical response. To obtain a different multiaxial condition in the off-axis layers of the unbalanced laminates, two angles were chosen based on Figure 2a, plotting the evolution of the λ ratios versus the angle θ, namely 30 and 60 degrees. It can be calculated that in the $[0^o/\theta]_{2s}$ lay-up the λ_{12} ratio is equal to 2.02 for $\theta=30^o$, whereas in the 60^o layers it equals 0.64. These values depict that in the case of the $[0^o/30^o]_{2s}$ laminates, the shear stresses τ_{12} are the dominant ones in the off-axis layers. On the other hand, the transverse stresses govern the stress state in the 60^o layers of the $[0^o/60^o]_{2s}$ laminates. In both cases, the stress along the fiber direction σ_1 is much lower than the unidirectional strength of the material in the off-axis layers, as it is depicted by looking at the λ_1 and λ_2 ratios in Figure 2a. Moreover, the same boundary conditions apply in both cases, with 0^o layers alternating the off-axis layers, proving that a direct comparison between the two laminates is allowed, letting the study of the matrix-

dominated behavior in the off-axis layers depend on either dominant shear or transverse stresses.

To examine the influence of balanced and unbalanced configurations on the mechanical response, $[0^o/\theta/0^o/-\theta]_s$ laminates with the same values of the angle θ were tested. In Figure 2b, the corresponding absolute biaxiality ratios are plotted. It can be calculated that λ_{12} equals 2.04 in the 30^o layers of the $[0^o/30^o/0^o/-30^o]_s$ laminates and 0.73 in the 60^o layers of the $[0^o/60^o/0^o/-60^o]_s$ laminates. Finally, to examine the impact of the relative number of off-axis layers θ with respect to the number of 0^o layers, 12-ply $[0^o/30^o/-30^o]_{2s}$ and $[0^o/60^o/-60^o]_{2s}$ laminates were tested, having also four 0^o layers, like the 8-ply $[0^o/\theta]_{2s}$ and $[0^o/\theta/0^o/-\theta]_s$ lay-ups. It can be calculated from CLT that λ_{12} equals 1.69 in the 30^o layers of the $[0^o/30^o/-30^o]_{2s}$ laminates. This shows that by increasing the number of the off-axis layers, λ_{12} drops, therefore the shear influence has the tendency to decrease. Nevertheless, the behavior remains shear-dominated. This phenomenon diminishes by increasing θ. In the 60^o layers of the $[0^o/60^o/-60^o]_{2s}$ laminates, λ_{12} equals 0.73, being similar with the $[0^o/60^o]_{2s}$ and $[0^o/60^o/0^o/-60^o]_s$ laminates.

3. Results

3.1. Comparison between balanced and unbalanced stacking sequences

The mechanical properties of the unbalanced lay-ups, $[0^o/30^o]_{2s}$ and $[0^o/60^o]_{2s}$, have been already presented in [25]. It was found that the $[0^o/30^o]_{2s}$ laminates lead to an average ultimate strength σ_{ult} of 1375 MPa and an elastic modulus of 78.2 GPa (in the undamaged state), whereas the failure stress of the $[0^o/60^o]_{2s}$ was 1318 MPa and the corresponding modulus equal to 74.1 GPa. A higher strength would be calculated also theoretically for the $[0^o/30^o]_{2s}$ laminates due to the less inclined off-axis layers with respect to the loading direction. In Figure 3, the experimental σ_{xx} stress-ε_{xx} strain curve of the $[0^o/30^o]_{2s}$ laminates (with x corresponding to the loading direction) is plotted, together with the respective linear curve, drawn by calculating the stiffness in the 0.001-0.003 ε_{xx} strain range. It is clear that no stiffness degradation occurs. On the contrary, the stiffness has the tendency to increase [33].

Moreover, as seen in [25], matrix cracking is not always the initial damage mode occurring.

Specifically, it was found that edge delaminations occurred before any matrix cracking in the $[0^o/30^o]_{2s}$ laminates. Delaminations were monitored after 1000 MPa applied stress (75% of σ_{ult}) which increased in size and number by increasing the load. Characteristic microscopy images are shown in Figures 4a and 4b at stress levels equal to 80% and 87% of σ_{ult} respectively. Initially outer-ply delaminations between the external 0^o and the adjacent 30^o layers were developed (Figure 4a). The change in the stress and displacement field resulting from these delaminations led to multiple matrix cracking of the single 30^o (thin) layers and consequently to inner-ply delaminations (Figure 4b). These delaminations were followed by fiber breakage resulting in final failure.

To compare the $[0^o/30^o]_{2s}$ with the $[0^o/30^o/0^o/-30^o]_s$ laminates, in Figure 5 the stress σ_{xx}-longitudinal strain ε_{xx} and stress σ_{xx}-transverse strain ε_{yy} curves are plotted. As a first remark, the balanced laminates lead to an average strength of 1057 MPa, being equal to only 76.9% of the strength of the unbalanced $[0^o/30^o]_{2s}$ laminates. However, the balanced laminates are stiffer than the unbalanced ones, with an average Young's modulus equal to 89.1 GPa, with no stiffening observed in this case. Moreover, even if the balanced laminates are characterized by a lower longitudinal strain to failure, the transverse strain is much higher than in the unbalanced laminates, explaining the interesting difference in Poisson's ratios. Specifically, ν_{xy} was found to be equal to 0.51 for the $[0^o/30^o]_{2s}$ laminates, whereas it reached values higher than 1, namely 1.06, in the balanced $[0^o/30^o/0^o/-30^o]_s$ laminates (values confirmed by CLT).

Interestingly, also the damage scenario showed differences in the balanced laminates. The high shear stresses in the off-axis layers of the $[0^o/30^o/0^o/-30^o]_s$ laminates led also in this case to interlaminar delaminations prior to matrix cracking. However, this time delaminations initiated between the inner layers of the laminate. In this case, for all samples tested, a first delamination appeared between the inner unidirectional 0^o layer and the off-axis (-30^o) layer, at a stress level much lower than in the unbalanced laminates, equal to 65% of σ_{ult}. The delamination increased in length, leading to very early fiber breakage in the inner 0^o layer, at the tip of the previously formed delamination, at around 69% of σ_{ult} (Figure 6a). Near the fiber breakage, matrix cracking then appeared in the middle double (-30^o)

(thick) layer at a stress equal to 72% of σ_{ult} (Figure 6b), leading afterwards to delamination and fiber breakage along the opposite (-30°)/0° interface when the stress reached 75% of σ_{ult} (Figure 6c). Close to final failure, at a stress equal to 90% of σ_{ult}, delamination between the outer 0° and 30° layers appeared (Figure 6d), leading to final fiber breaks and failure. In Figure 7 the average delamination crack growth in the balanced and unbalanced laminates during loading is shown. It is obvious that in the balanced laminates delaminations occur at much lower stresses. The inner-ply delaminations saturate during loading while the outer-ply ones increase with a high rate leading to final failure.

A comparison of the cumulative AE activity between the balanced and unbalanced laminates is shown in Figure 8. A clear deviation between the two curves is shown after 650 MPa stress, corresponding to the stress level at which delaminations started appearing in the balanced laminates. The slope of the AE curve drops after 850 MPa stress, following the saturation of the delaminations, as shown in Figure 7. After 900 MPa stress, AE initiates again with a high rate, indicating the final delaminations and the upcoming catastrophic failure. In the unbalanced laminates, an exponential-like increase of the AE events appears, presenting a high rate after 1000 MPa stress, close to which initial delaminations were monitored. However, AE monitoring revealed the initiation of microscale damage prior to the appearance of delaminations in both laminates at a relatively early stress level. Specifically, AE onset appeared at around 275 MPa stress in the unbalanced laminates, attributed most probably to intralaminar shear debondings due to the increasing shear. In the balanced laminates, AE initiated at around 360 MPa on average. In Figure 9 the σ_2 and τ_{12} stress distribution through the thickness of the laminates during AE onset, as calculated by CLT, is plotted. It is remarkable that in both laminates, AE initiates when the shear stress in the off-axis layers, τ_{12}, reaches a value between 27-30 MPa, being half of the material shear strength. Internal shear damage occurs after this stress, which though does not lead to matrix cracks, even if this would be the prediction of most damage models. According to [24], the tensile transverse stresses σ_2 acting in the 30° layers of the $[0°/30°]_{2s}$ laminates would eventually lead to matrix cracks but this only happens late in the test, after initiation and growth of delaminations.

To explain the difference in the strength and the damage scenario between the two laminates, one should look at the stress states developed during testing. Both laminates are shear-dominated, leading to AE initiation at a similar shear stress level in the off-axis layers. However, the balanced laminates lead to interlaminar delaminations at a quite lower stress level. This can be attributed on one hand to the fact that σ_2 is compressive in their off-axis layers. The combination of compressive transverse stresses with shear stresses appears detrimental for the mechanical behavior. To explain this further, the interlaminar normal and shear stresses developed close to the free edge of the laminates were calculated, by using an accurate analytical approach based on variational analysis [34], [35]. For this analysis the ply was assumed transversely isotropic with moduli $E_3=E_2$ and $G_{13}=G_{23}=G_{12}$, and Poisson's ratios $\nu_{13}=\nu_{12}$ and $\nu_{23}=0.4$. In Figure 10, the through-thickness interlaminar stresses σ_{zz} and τ_{xz} developed on the free edge are plotted for 700 MPa stress, corresponding to the stress level at which delaminations appeared for the first time in the balanced laminates. It is evident from Figure 10 that the balanced laminates are characterized by higher interlaminar stresses on their edge, proposing a possible explanation for the higher sensitivity to the appearance of delaminations. It should be mentioned at this point that the fracture toughness for Mode I delaminations G_I for that particular material was experimentally obtained and equals 104 N/m on average.

In Figure 11, the evolution of the Poisson's ratio ν_{xy} for the two laminates is plotted versus the applied stress. For the calculation of the Poisson's ratio, the longitudinal ε_{xx} and transverse ε_{yy} strains, obtained by the DIC measurements, were used. For the unbalanced laminates, ν_{xy} presents a more stable evolution in lower values, with a small increasing tendency until the stress level at which delaminations appear, followed by a little decrease after this point. On the other hand, in the balanced laminates, a continuously increasing tendency is recorded. Interestingly, two jumps on the curve of the Poisson's ratio are recorded close to the stress levels at which delaminations occurred. This shows the potential of simple mechanical properties, like the Poisson's ratio, to be used as damage indices.

The DIC technique could also indicate differences in the strain pattern between the unbalanced and

balanced lay-ups. In Figure 12 a comparison is shown by plotting the distribution of the transverse strains ε_{yy} on the surface of the specimens at a stress level equal to 650 MPa, corresponding to just a lower stress than the appearance of delaminations in the balanced laminates. The higher ε_{yy} strains in the balanced laminates are apparent (Figure 12b). Moreover, the strain distribution in the balanced lay-up follows always a certain pattern, with quite constant values on the greatest part of the surface but with lower strains close to the edges. This is not the case in the unbalanced lay-up (Figure 12a).

Furthermore, the DIC technique can prove its potential for damage indication. This can be achieved by using the sigma parameter, measured in pixels, representing the confidence interval for the match at any point of the correlated area with respect to the reference image referring to the unloaded state. Characteristic examples are presented in Figure 13. In Figure 13a, the sigma distribution on the surface of a $[0^o/30^o]_{2s}$ laminate is plotted at around 1030 MPa stress, and in Figure 13b the subsequent image after the occurrence of delamination is shown, both derived at the area of the monitored delamination. Similarly, Figures 13c and 13d plot the distribution of the sigma value before and after the delamination occurring in a $[0^o/30^o/0^o/-30^o]_s$ laminate at around 700 MPa stress. In both cases, a sudden change of the sigma pattern is obvious after the occurrence of delamination, corresponding to out-of-plane movements, which consequently lead to high sigma values. This proves that the DIC can, at least on a qualitative level, indicate the appearance of internal damage, even if it only offers surface measurements. Moreover, taking advantage of the DIC 3D analysis, the displacement w, measured in mm, in the out-of-plane direction z, can be also measured. When a delamination occurs, the DIC measurements prove to be sensitive enough to small out-of-plane movements, indicating the damage appearing. A characteristic example is shown in Figure 14, in which the average evolution of w on the total surface of one $[0^o/30^o/0^o/-30^o]_s$ specimen versus the stress is plotted. Interestingly, three jumps appear in the displacement-stress curve, corresponding to the stress levels at which delaminations were monitored. At the same time, the measured w values provide an approximate quantitative indication of the occurring delaminations, corresponding interestingly to their total crack opening.

3.2. Influence of different multiaxiality on the mechanical response and fracture process

To study the influence of dissimilar multiaxial stresses in the off-axis layers of the carbon/epoxy laminates, the previous results are compared with those of the $[0^o/60^o]_{2s}$ and $[0^o/60^o/0^o/-60^o]_s$ laminates. In these cases, the transverse stresses dominate the stress state in the off-axis layers. In Figures 15a and 15b, the stress σ_{xx}-longitudinal strain ε_{xx} and stress σ_{xx}-transverse strain ε_{yy} curves are plotted. As mentioned earlier, the unbalanced $[0^o/60^o]_{2s}$ laminates lead to an average tensile strength of 1318 MPa and a stiffness of 74.1 GPa and this reduction compared to the $[0^o/30^o]_{2s}$ laminates comes in agreement with most of the failure criteria, due to the higher inclination of the fibers in the off-axis layers with respect to the loading direction. Nevertheless, the decrease in strength (≈4.1%) and stiffness (≈5.2%) is relatively small when changing the angle from 30^o to 60^o in the off-axis layers of the unbalanced laminate configuration. Moving to the balanced configuration, the average failure stress of the $[0^o/60^o/0^o/-60^o]_s$ laminates reaches 1213 MPa and the corresponding stiffness is equal to 76.9 GPa. As a first comment, this means that also in this case the balanced configuration leads to a reduction in the obtained strength and an increase in the measured stiffness for the same off-axis angle θ. However, in this case, the strength is only reduced by 8.0%, in comparison to the 23.1% reduction that was obtained when the balanced laminates with a 30^o angle were compared to the corresponding unbalanced laminates. Nevertheless, the most interesting finding concerns the comparison between the balanced $[0^o/30^o/0^o/-30^o]_s$ and $[0^o/60^o/0^o/-60^o]_s$ laminates. It is obvious that by increasing the angle from 30^o to 60^o in the balanced lay-up, the average strength increases from 1057 MPa to 1213 MPa, corresponding to a 14.8% increase. This disagrees with the failure criteria used in literature, which would predict the inverse phenomenon due to the smaller off-axis angle of the $[0^o/30^o/0^o/-30^o]_s$ laminates, showing that shear damage mechanisms are detrimental in the carbon/epoxy material. However, higher stiffness is always obtained when the off-axis angle decreases, in the same way as failure theories would also predict.

Moving to the fracture process, matrix cracking in the off-axis layers was always the primary damage

mode occurring during loading. The dominant transverse stresses and strains created in both cases the ideal conditions for the matrix cracking to occur. Matrix cracking was followed by outer-ply interlaminar delaminations between the external 0^o and the adjacent 60^o layers, but only very close to final failure. Despite the similar mechanical properties obtained for the two laminates, differences concerning the amount of developing damage were observed. In Figure 16 the evolution of the matrix crack density is plotted, measured in the thin (single) and thick (double layer in the middle of the laminate) off-axis layers for both lay-ups. The crack density is expressed in cracks/mm and it concerns the total amount of cracks monitored along the gauge length of all tested specimens. It is obvious from Figure 16 that in both cases the crack density is constantly bigger for the thin layers in comparison to the middle thick one. Moreover, the balanced laminates lead to significantly higher crack densities than the unbalanced ones. Towards the end of the test, the balanced laminates reach values of 3 cracks/mm in their thin layers, whereas the unbalanced laminates do not exceed a crack density of 1.5 cracks/mm. It is also characteristic that in the $[0^o/60^o]_{2s}$ laminates the crack density reaches a saturation point, after which no newly created cracks are monitored. However, this is not the case for the $[0^o/60^o/0^o/-60^o]_s$ laminates, in which a continuous increase of the matrix cracks is recorded, something that was similarly observed in [36]. Additionally, very important is the fact that the initiation of the matrix cracks occurs at a lower stress level in the balanced laminates. Specifically, at around 425 MPa stress (35% of σ_{ult}) the first matrix cracks in the thick double (-60^o) layer occur, whereas in the unbalanced laminates the initiation of the matrix cracks occurs only at around 600 MPa stress (45% of σ_{ult}). Moreover, in the case of the unbalanced laminates the occurrence of the matrix cracks takes place simultaneously in the thin and thick off-axis layers, whereas in the balanced laminates matrix cracking occurs first in the thick (-60^o) layer even though it is characterized by lower matrix crack density in comparison to the thin layers. In Figures 17 and 18, characteristic microscopy images are presented at indicative stress levels.

In Figure 19, the Poisson's ratio evolution for the laminates with a 60^o off-axis layer is plotted versus the stress. The v_{xy} values, measured by DIC, are more stable in the beginning of the test and much lower

in comparison to the laminates with 30° off-axis layers, corresponding to theoretically calculated values from CLT. However, as damage accumulates, the ν_{xy} values start decreasing in both cases. Interestingly, this decrease initiates at a stress level a bit lower than the one in which matrix cracks were microscopically visible. The above findings lead to the deduction that the Poisson's ratio can, at least in a qualitative manner, provide information for the transition from limited to more severe damage, probably even prior to any visible fracture.

In Figure 20 the cumulative AE activity recorded for both the balanced and the unbalanced laminates is plotted. It is obvious also in this case that the balanced $[0^o/60^o/0^o/-60^o]_s$ laminates are characterized by a more intense AE activity, corresponding to the higher matrix crack density. Considering the AE onset, in both laminates AE initiated at an applied stress equal to approximately 400 MPa, corresponding in both cases to a transverse stress σ_2 of almost 38 MPa in the off-axis 60° and (-60°) layers. It is important to mention that both for the balanced and the unbalanced laminates, an earlier AE onset was constantly registered for an off-axis angle equal to 30°, like shown in Figure 8. The earlier AE detection in laminates consisting of 30° plies can be explained by the developing shear friction and intralaminar debondings owing to the high shear stresses occurring in their off-axis layers, justifying also the exponential increase of the AE events until final failure. To verify this assumption, in Figure 21 post-mortem microscopy images from a section in the middle of the $[0^o/30^o]_{2s}$ and $[0^o/60^o]_{2s}$ laminates at a stress equal to 400 MPa are shown. It is obvious that in the $[0^o/30^o]_{2s}$ laminates matrix-fiber debondings have occurred, logically attributed to the high shear stresses in the 30° layers, whilst clear surfaces still appear in the $[0^o/60^o]_{2s}$ laminates with no obvious intralaminar decohesions.

In Figure 22, the in-plane σ_2 and τ_{12} stress distribution in the $[0^o/60^o]_{2s}$ and $[0^o/60^o/0^o/-60^o]_s$ laminates is plotted during the application of 400 MPa stress. It is remarkable that in the balanced laminates initial matrix cracks were microscopically observed at a stress of 425 MPa, being close to the AE onset level. The early damage assessment offered by AE was more obvious in the unbalanced laminates, since first matrix cracks were observed at 600 MPa stress, quite later than the AE onset. This is evidence of a more

brittle behavior of the balanced laminates, with microcracks requiring less energy to propagate and to form visible matrix cracks. Furthermore, the simultaneous matrix cracking formation in all off-axis layers can explain the quite linear AE activity of the unbalanced laminates during the matrix cracking stage. In Figure 23, the interlaminar stresses σ_{zz} and τ_{xz} on the edge of the laminates are plotted for 425 MPa stress. Similar distribution is observed in both laminates with much lower values than in the case of the 30^o off-axis angle, explaining the lower probability for delaminations to occur in laminates with 60^o plies.

It is important to mention at this point that in order to confirm that the findings of the microscope along one edge of the specimens were not caused by an unbalanced load introduction, one USB microscope was used for damage monitoring on both sides of the samples during all test intervals, confirming similar damage progression. Moreover, in order to examine whether the observed damage was driven only by free edge effects and to obtain an indication of the mid-plane damage state of the material, post-mortem monitoring was performed at least in two load steps in all laminates under consideration. The through-thickness damage findings at the edge of the laminates were confirmed by the damage in the bulk material, especially regarding the appearance and size of delaminations in all tested specimens. In order to obtain an indication of the length of the matrix cracks during the static loading as well, one specimen both from the $[0^o/60^o/0^o/\text{-}60^o]_s$ and from the $[0^o/60^o]_{2s}$ laminates was loaded until a stress equal to 60% of the corresponding σ_{ult}. The specimen was afterwards cut in the middle, remaining with a width equal to 12.5 mm, and was then mounted back on the test bench after polishing. It was then loaded again until the same stress level in order to observe the developed damage state inside the material. Surprisingly, no matrix cracks were observed in the off-axis layers of the $[0^o/60^o]_{2s}$ laminate, meaning that the cracks monitored at the edge had not yet propagated along the total width. On the other hand, matrix cracks were observed in the mid-plane of the balanced $[0^o/60^o/0^o/\text{-}60^o]_s$ laminate, though with a lower crack density equal to 0.5 cracks/mm. Similar monitoring in the $[0^o/30^o/0^o/\text{-}30^o]_s$ and $[0^o/30^o]_{2s}$ laminates at a stress equal to 80% of σ_{ult} proved that only delaminations were developed in the mid-plane of the specimens with an absence of matrix cracks.

3.3. Influence of the number of off-axis layers on the mechanical response

To account for the influence of the number of off-axis layers on the mechanical response, in Figures 24a and 24b, a comparison of the average strength and stiffness obtained for the 12-ply and 8-ply balanced laminates for both θ values is respectively presented. By comparing the two 12-ply laminates, a higher strength can be observed for the $[0^o/30^o/-30^o]_{2s}$ case, with an increase of 8.5% in comparison to the $[0^o/60^o/-60^o]_{2s}$ laminates. A significant increase in stiffness, equal to 44.8%, is observed when decreasing the angle from 60^o to 30^o in the 12-ply $[0^o/\theta/-\theta]_{2s}$ laminates. The biggest influence of the number of the off-axis layers can be seen for an off-axis angle θ equal to 60^o. Specifically, a decrease in strength equal to 26.5% and a decrease in stiffness equaling 32.9% is obtained when moving from the 8-ply $[0^o/60^o/0^o/-60^o]_s$ laminates to the 12-ply $[0^o/60^o/-60^o]_{2s}$ laminates. Undoubtedly, this is a normal consequence, since the number of off-axis layers is increased with respect to the 0^o layers, which can carry most of the loads. Nevertheless, this influence is reduced when moving to the 30^o angle. Definitely, also in this occassion, a decrease of 8.5% in strength and a decrease of 16.2% in stiffness is obtained when moving from the 8-ply $[0^o/30^o/0^o/-30^o]_s$ lay-up to the 12-ply $[0^o/30^o/-30^o]_{2s}$ laminates but the drop is significantly lower. In both cases shear is dominant in the off-axis layers and shear-compression stress conditions emerge, however the lay-up structure of the 12-ply laminates compensates to some extent for the bigger number of off-axis layers, as will be shown in the following. Furthermore, the Poisson's ratio ν_{xy} was found to be equal to 1.17 in the $[0^o/30^o/-30^o]_{2s}$ laminates and equal to 0.32 in the $[0^o/60^o/-60^o]_{2s}$ laminates.

Regarding hence the fracture process of the 12-ply laminates, similar response with the 8-ply lay-ups was observed for the same angle θ. Interlaminar delamination was the primary damage mode occurring in the $[0^o/30^o/-30^o]_{2s}$ laminates due to dominant shear stresses. However in this case the occurring delaminations between the inner layers saturated quickly, due to the multiple interfaces between the different plies, serving as potential points for the creation of new fracture phenomena and as obstacles for the propagation of the previously formed delaminations. Damage was localized in a certain region,

leading later to final delaminations and failure. Characteristic microscopy images showing the development of the fracture path are presented in Figure 25. In the 12-ply $[0^o/30^o/-30^o]_{2s}$ laminates the first delamination appeared at a stress equal to 485 MPa on average. In Figure 26a the σ_2 and τ_{12} through-thickness distribution at 485 MPa stress is shown, corresponding to a compressive σ_2 stress equal to -30 MPa and a τ_{12} equal to 51 MPa in the off-axis layers. In the 8-ply $[0^o/30^o/0^o/-30^o]_s$ laminates, initial delaminations appeared when τ_{12} reached 57 MPa, being somehow higher than in the $[0^o/30^o/-30^o]_{2s}$ laminates. This can be explained by the higher σ_2 stresses developed in the latter case, confirming the detrimental influence of combining shear with compression, as well as by the very high interlaminar stresses at the edges of the laminate (y=-12.5 mm and 12.5 mm), plotted in Figure 26b.

The balanced 12-ply $[0^o/60^o/-60^o]_{2s}$ laminates presented a similar fracture process with the 8-ply $[0^o/60^o/0^o/-60^o]_s$ laminates, with matrix cracks appearing first in the middle double $(-60^o)/(-60^o)$ (thick) layer at a stress level equal to 35% of σ_{ult} (310 MPa). Only after a stress level equal to 50% of σ_{ult}, matrix cracks were monitored in the rest of the off-axis layers. The matrix crack density increased, and interlaminar delaminations started appearing at 85% of σ_{ult}, increasing in length and leading to final failure. It is characteristic that while in the previous cases matrix cracks were developed along the entire thickness of the layers, in this case also random cracks with a shorter length appeared. In Figure 27 characteristic damage state images are shown and in Figure 28 the matrix crack density evolution is plotted. It is noteworthy that the crack densities measured for the 12-ply laminates were the highest ones recorded, reaching even 3.5 cracks/mm towards the end of the test, proving a certain influence of the number of off-axis layers. It can be calculated that when first cracks appeared in the $[0^o/60^o/-60^o]_{2s}$ laminates, the transverse stress σ_2 in the 60^o plies was equal to around 40 MPa, corresponding perfectly to the local stress values when matrix cracking first appeared in the $[0^o/60^o/0^o/-60^o]_s$ samples.

Also in the case of the 12-ply lay-ups, the mid-plane damage state was quite similar to the damage monitored at the edge of the laminates, with relatively lower mid-plane matrix crack density in the $[0^o/60^o/-60^o]_{2s}$ laminates, at least when the applied stress was equal to 60% of σ_{ult}. As a last comment, in

the $[0^o/30^o/-30^o]_{2s}$ laminates, AE initiated when the shear stress τ_{12} reached 30 MPa in the off-axis layers. In the $[0^o/60^o/-60^o]_{2s}$ laminates, AE initiated when the transverse stress σ_2 exceeded 37 MPa. Taking into account these values and the ones obtained for the previous laminates, it can be concluded that the initiation of AE is in any case related to certain stress levels developed in the laminate, independently of the stacking sequence. The accumulation of AE and the fracture process are however linked to the lay-up, leading to different mechanical properties.

4. Conclusions

In this study, the influence of three parameters, i.e. multiaxiality, unbalanced stacking sequences and number of off-axis layers on the mechanical response and the damage development of carbon/epoxy laminates was investigated. 8-ply unbalanced $[0^o/\theta]_{2s}$, 8-ply balanced $[0^o/\theta/0^o/-\theta]_s$ and 12-ply balanced $[0^o/\theta/-\theta]_{2s}$ laminates for two different θ values, 30^o and 60^o, were therefore tested. It was observed that when shear is dominant in the off-axis layers of the composite laminate, interlaminar delaminations occur even prior to matrix cracking, driven by in-plane shear and high out-of-plane interlaminar stresses at the edges of the laminates. The potential of the unbalanced stacking sequences was exploited. Unbalanced laminates exhibited in all cases improved strength and a better damage response, either with delaminations appearing at higher stress levels or with lower matrix crack densities during testing. The effect of the number of the off-axis layers was also analyzed, showing that multiple interfaces lead to severe concentrated damage and to higher crack densities. Nevertheless, increasing the number of off-axis layers in laminates with dominant shear stresses seemed to compensate to some extent the impact of the reduced strength of the off-axis plies by leading to rapid saturation of short delamination lengths due to the formed fracture path and the corresponding stress redistribution.

In-situ microscopy offered detailed damage investigations during testing. DIC provided damage indices and AE proved its potential for early damage identification. It was noticed that AE initiated in all cases when the dominant stress component reached a certain value during testing, showing the

dependence of microscale damage development on certain stress states. The fracture development and the final mechanical response was nevertheless always dependent on the specific stacking sequence. Finally, even simple mechanical properties, like for instance the Poisson's ratio, proved their potential to be used as damage indices, at least in a qualitative manner.

Acknowledgements

The work leading to this publication has been partially funded by the SBO project "M3Strength", which fits in the MacroModelMat (M3) research program, coordinated by Siemens (Siemens PLM software, Belgium) and funded by SIM (Strategic Initiative Materials in Flanders) and VLAIO (Flanders Innovation & Entrepreneurship Agency). The authors gratefully acknowledge the material suppliers Mitsubishi Chemical Corporation and Honda R&D Co., Ltd. and would like to thank the financial support of the Fonds Wetenschappelijk Onderzoek (FWO) research program "Multi-scale modelling and characterization of fatigue damage in unidirectionally reinforced polymer composites under multiaxial and variable-amplitude loading" (G.0090.15).

References

[1] M.J. Hinton, P.D. Soden, Predicting failure in composite laminates: the background to the exercise, Compos. Sci. Technol. 58 (7) (1998) 1001–1010.

[2] I.M. Daniel, Yield and failure criteria for composite materials under static and dynamic loading, Prog. Aerosp. Sci. 81 (2016) 18–25.

[3] Y. Chen, Y. Zhao, C. He, S. Ai, H. Lei, L. Tang, D. Fang, Yield and failure theory for unidirectional polymer-matrix composites, Compos. Part B Eng. 164 (2019) 612–619.

[4] R.M. Christensen, Stress based yield/failure criteria for fiber composites, Int. J. Solids Struct. 34 (5) (1997) 529–543.

[5] L.J. Hart-Smith, Predictions of the original and truncated maximum-strain failure models for certain fibrous composite laminates, Compos. Sci. Technol. 58 (7) (1998) 1151–1178.

[6] A. Puck, H. Schürmann, Failure analysis of FRP laminates by means of physically based phenomenological models, Compos. Sci. Technol. 62 (12–13) (2002) 1633–1662.

[7] L.J. Hart-Smith, A re-examination of the analysis of in-plane matrix failures in fibrous composite laminates, Compos. Sci. Technol. 56 (2) (1996) 107–121.

[8] M. Shahverdi, A.P. Vassilopoulos, T. Keller, Mixed-mode quasi-static failure criteria for adhesively-bonded pultruded GFRP joints, Compos. Part A Appl. Sci. Manuf. 59 (2014) 45–56.

[9] R. Talreja, Damage and fatigue in composites – a personal account, Compos. Sci. Technol. 68 (13) (2008) 2585–2591.

[10] S.A. Elnekhaily, R. Talreja, Effect of axial shear and transverse tension on early failure events in unidirectional polymer matrix composites, Compos. Part A Appl. Sci. Manuf. 119 (2019) 275–282.

[11] A.S. Chen, F.L. Matthews, A review of multiaxial/biaxial loading tests for composite materials, Composites 24 (5) (1993) 395–406.

[12] D. Cai, J. Tang, G. Zhou, X. Wang, C. Li, V.V. Silberschmidt, Failure analysis of plain woven glass/epoxy laminates: Comparison of off-axis and biaxial tension loadings, Polym. Test. 60 (2017) 307–320.

[13] E. Totry, C. González, J. Llorca, Prediction of the failure locus of C/PEEK composites under transverse compression and longitudinal shear through computational micromechanics, Compos. Sci. Technol. 68 (15–16) (2008) 3128–3136.

[14] M. Hinton, A.S. Kaddour, P.D. Soden, Failure criteria in fibre reinforced polymer composites: the world-wide failure exercise, Elsevier, 2004.

[15] L.N. McCartney, Model to predict effects of triaxial loading on ply cracking in general symmetric laminates, Compos. Sci. Technol. 60 (12–13) (2000) 2255–2279.

[16] A. Turon, P.P. Camanho, J. Costa, C.G. Dávila, A damage model for the simulation of delamination in advanced composites under variable-mode loading, Mech. Mater. 38 (11) (2006) 1072–1089.

[17] J. Varna, L. Berglund, Multiple transverse cracking and stiffness reduction in cross-ply laminates, J. Compos. Technol. Res. 13 (2) (1991) 97–106.

[18] J. Reiner, M. Veidt, M. Dargusch, L. Gross, A progressive analysis of matrix cracking-induced delamination in composite laminates using an advanced phantom node method, J. Compos. Mater. 51 (20) (2017) 2933–2947.

[19] B. Mohammadi, M. Rohanifar, D. Salimi-Majd, A. Farrokhabadi, Micromechanical prediction of damage due to transverse ply cracking under fatigue loading in composite laminates, J. Reinf. Plast. Compos. 36 (5) (2017) 377–395.

[20] H. Ben Kahla, Z. Ayadi, F. Edgren, A. Pupurs, J. Varna, Statistical model for initiation governed intralaminar cracking in composite laminates during tensile quasi-static and cyclic tests, Int. J. Fatigue 116 (2018) 1–12.

[21] M. Quaresimin, P.A. Carraro, Damage initiation and evolution in glass/epoxy tubes subjected to combined tension-torsion fatigue loading, Int. J. Fatigue 63 (2014) 25–35.

[22] C.V. Singh, R. Talreja, A synergistic damage mechanics approach to mechanical response of composite laminates with ply cracks, J. Compos. Mater. 47 (20–21) (2013) 2475–2501.

[23] J. Montesano, C.V. Singh, A synergistic damage mechanics based multiscale model for composite

laminates subjected to multiaxial strains, Mech. Mater. 83 (2015) 72–89.

[24] J. Varna, R. Joffe, N.V. Akshantala, R. Talreja, Damage in composite laminates with off-axis plies, Compos. Sci. Technol. 59 (14) (1999) 2139–2147.

[25] K.A. Kalteremidou, B. Murray, E. Tsangouri, D. Aggelis, D. Van Hemelrijck, L. Pyl, Multiaxial damage characterization of carbon/epoxy angle-ply laminates under static tension by combining in situ microscopy with acoustic emission, Appl. Sci. 8 (11) (2018) 2021.

[26] C.B. York, S.F.M. De Almeida, On extension-shearing bending-twisting coupled laminates, Compos. Struct. 164 (2017) 10–22.

[27] Y.H.N. Kim, S. Ko, W.S. Lay, J. Tian, P. Chang, S.U. Thielk, H.J. Bang, J. Yang, Effects of shallow biangle, thin-ply laminates on structural performance of composite wings, AIAA J. 55 (6) (2017) 2086–2092.

[28] D.N. Betts, H.A. Kim, C.R. Bowen, D.J. Inman, Optimal configurations of bistable piezo-composites for energy harvesting, Appl. Phys. Lett. 100 (2012) 11:114104.

[29] R. Gutkin, C.J. Green, S. Vangrattanachai, S.T. Pinho, P. Robinson, P.T. Curtis, On acoustic emission for failure investigation in CFRP: Pattern recognition and peak frequency analyses, Mech. Syst. Signal Process. 25 (4) (2011) 1393–1407.

[30] N. Godin, P. Reynaud, G. Fantozzi, Contribution of AE analysis in order to evaluate time to failure of ceramic matrix composites, Eng. Fract. Mech. 210 (2019) 452–469.

[31] R. De Oliveira, A.T. Marques, Health monitoring of FRP using acoustic emission and artificial neural networks, Comput. Struct. 86 (3–5) (2008) 367–373.

[32] M. Quaresimin, P.A. Carraro, L.P. Mikkelsen, N. Lucato, L. Vivian, P. Brøndsted, B.F. Sørensen, J. Varna, R. Talreja, Damage evolution under cyclic multiaxial stress state: A comparative analysis between glass/epoxy laminates and tubes, Compos. Part B Eng. 61 (2014) 282–290.

[33] G. Zhou, J.H. Byun, S.B. Lee, J.W. Yi, W. Lee, S.K. Lee, B.S. Kim, J.K. Park, S.G. Lee, L. He, Nano structural analysis on stiffening phenomena of PAN-based carbon fibers during tensile deformation, Carbon Lett 76 (2014) 232–239.

[34] M. Hajikazemi, W. Van Paepegem, A variational model for free-edge interlaminar stress analysis in general symmetric and thin-ply composite laminates, Compos. Struct. 184 (2018) 443–451.

[35] M. Hajikazemi, W. Van Paepegem, Variational analysis of free-edge stress and displacement fields in general un-symmetric and thin-ply laminates under in-plane, bending and thermal loading, Compos. Part A Appl. Sci. Manuf. 113 (2018) 220–232.

[36] P. Johnson, F.K. Chang, Characterization of matrix crack-induced laminate failure-Part I: Experiments, J. Compos. Mater. 35 (22) (2001) 2009–2035.

Figures

Figure 1

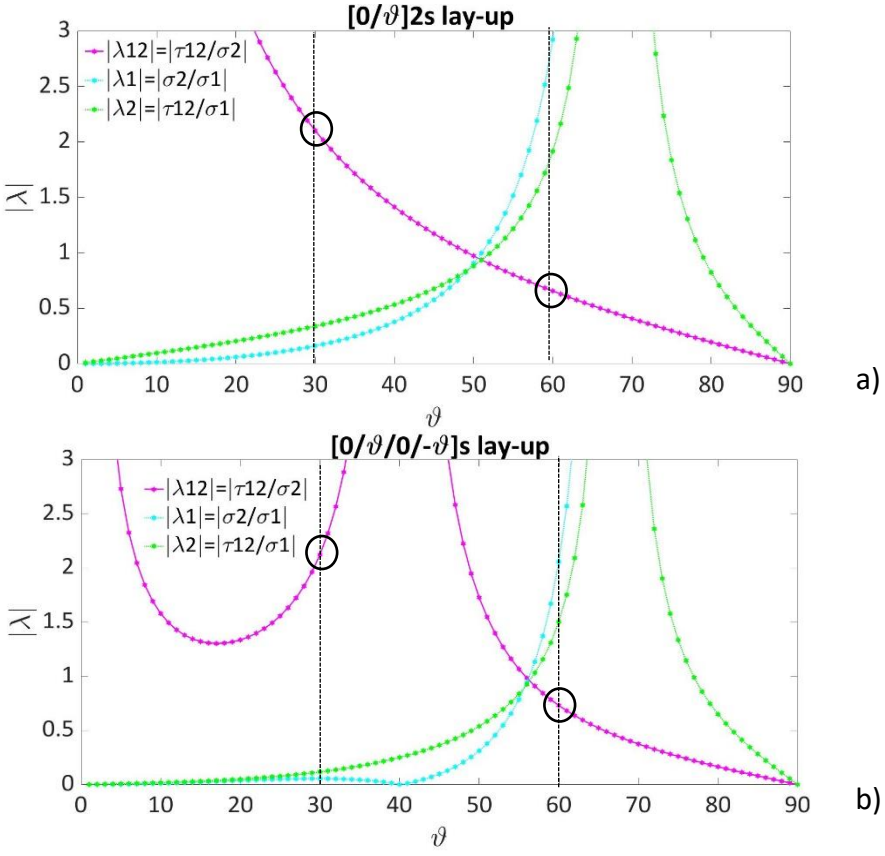

Figure 2

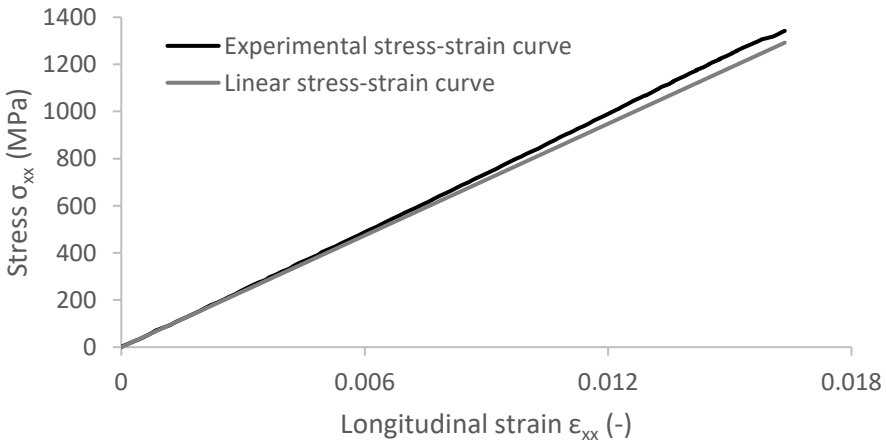

Figure 3

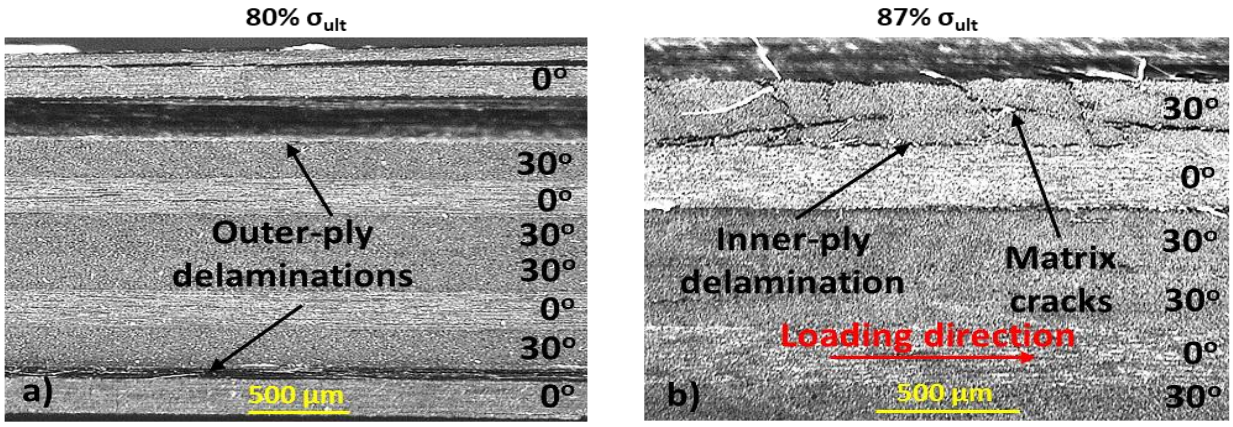

Figure 4

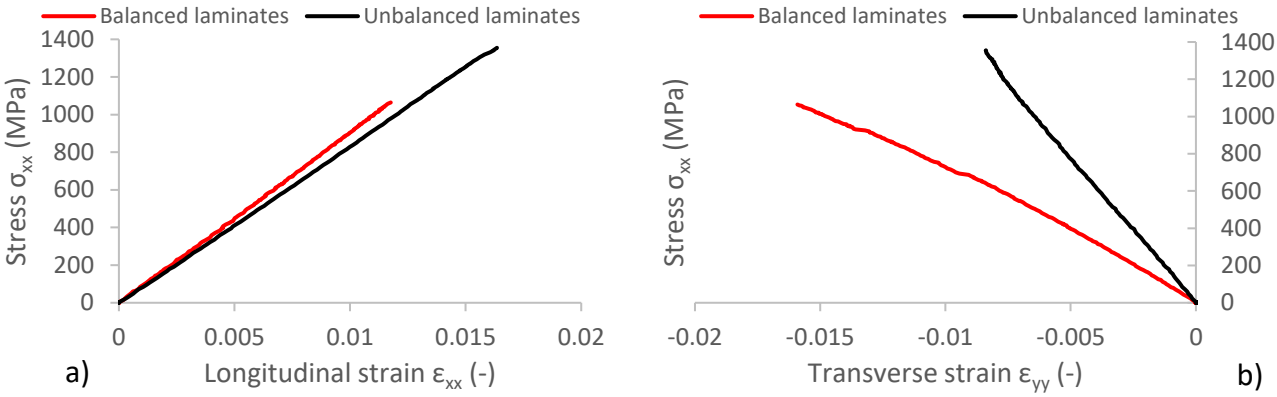

Figure 5

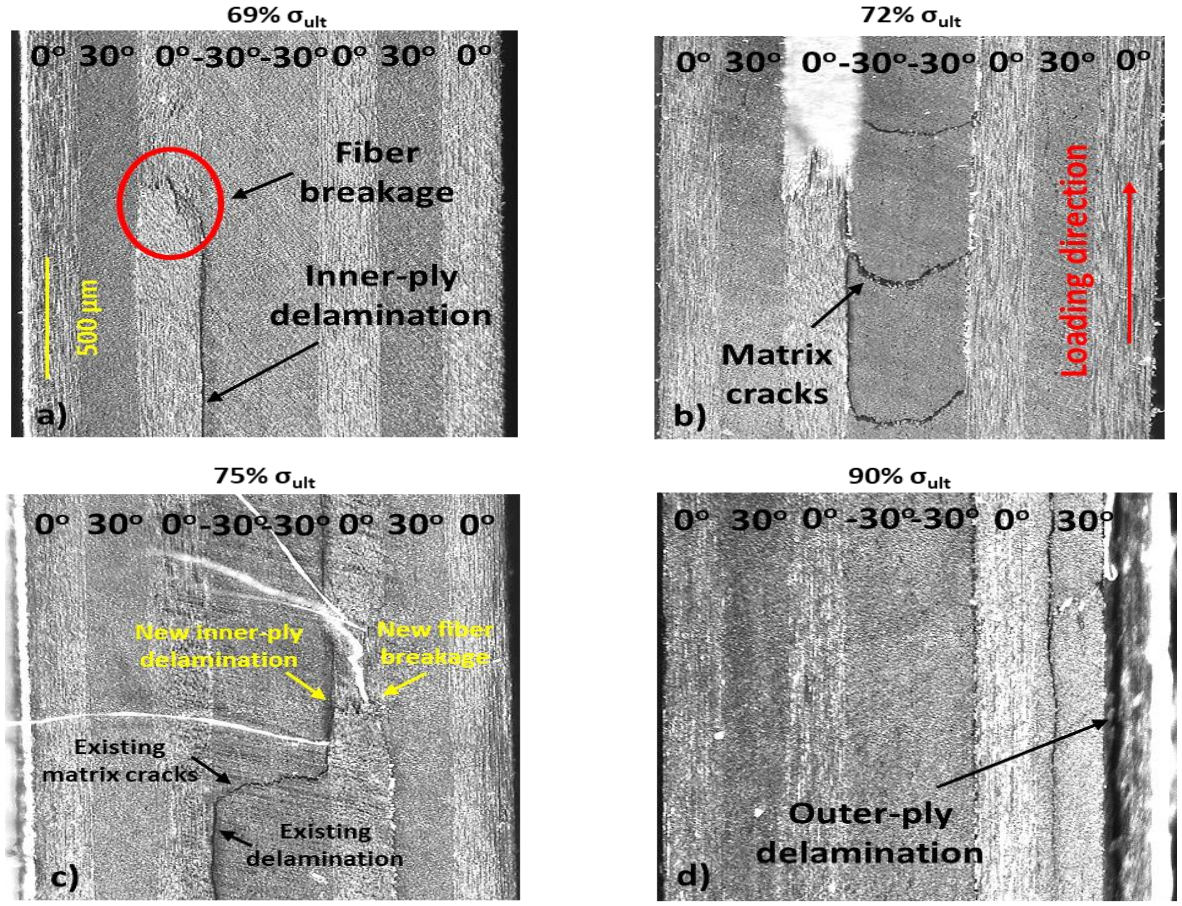

Figure 6

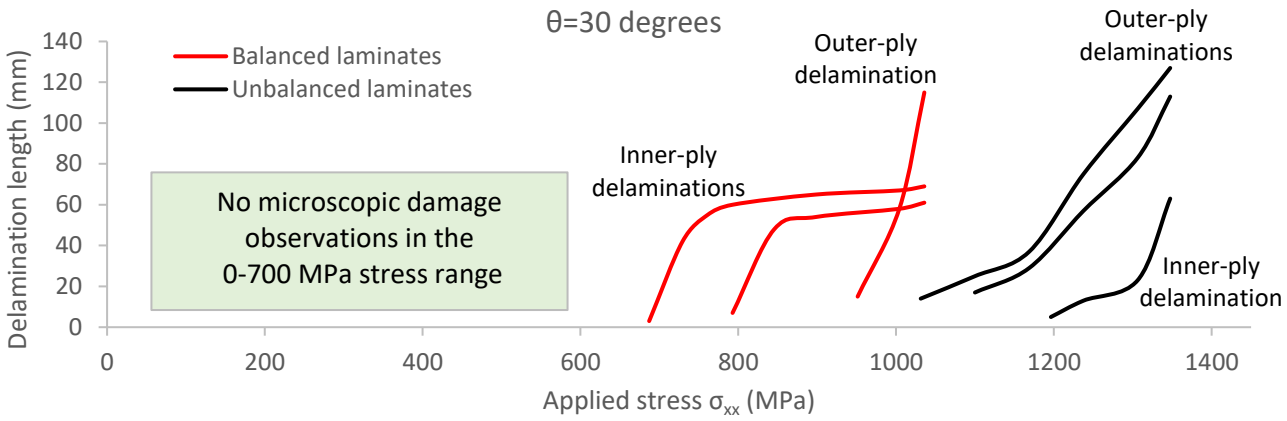

Figure 7

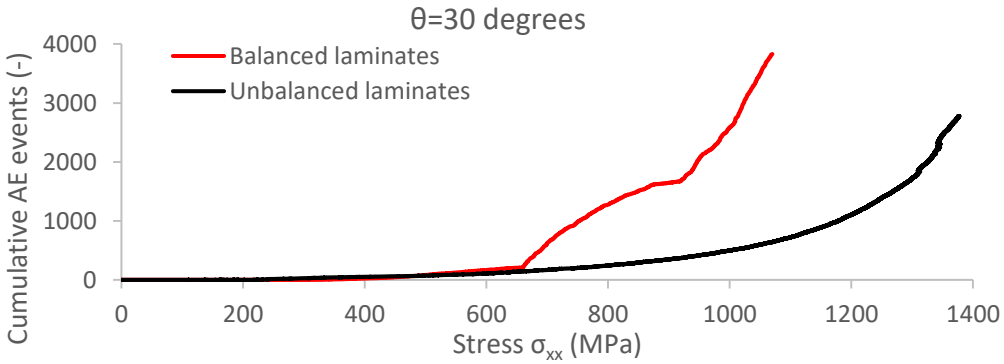

Figure 8

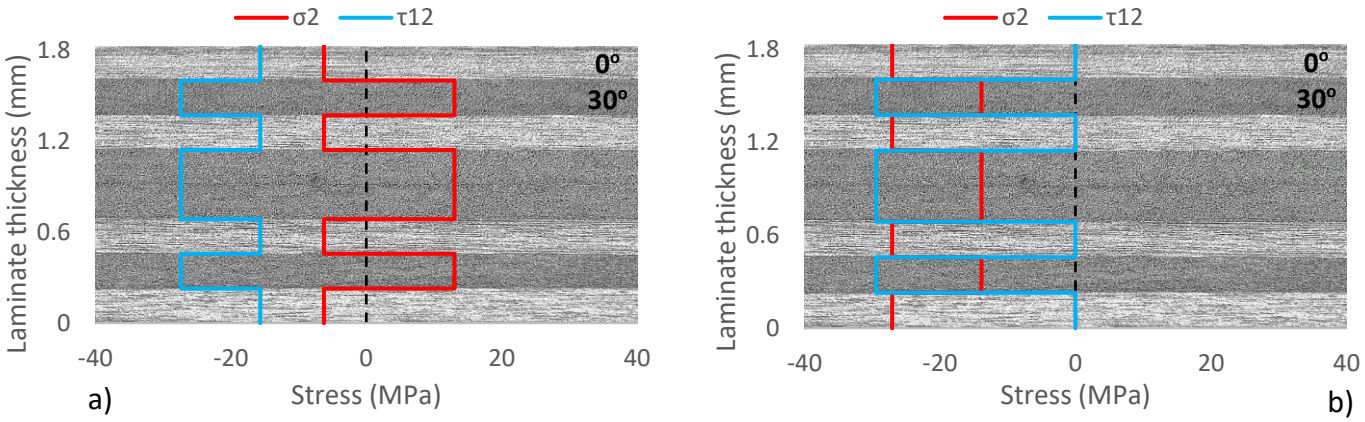

Figure 9

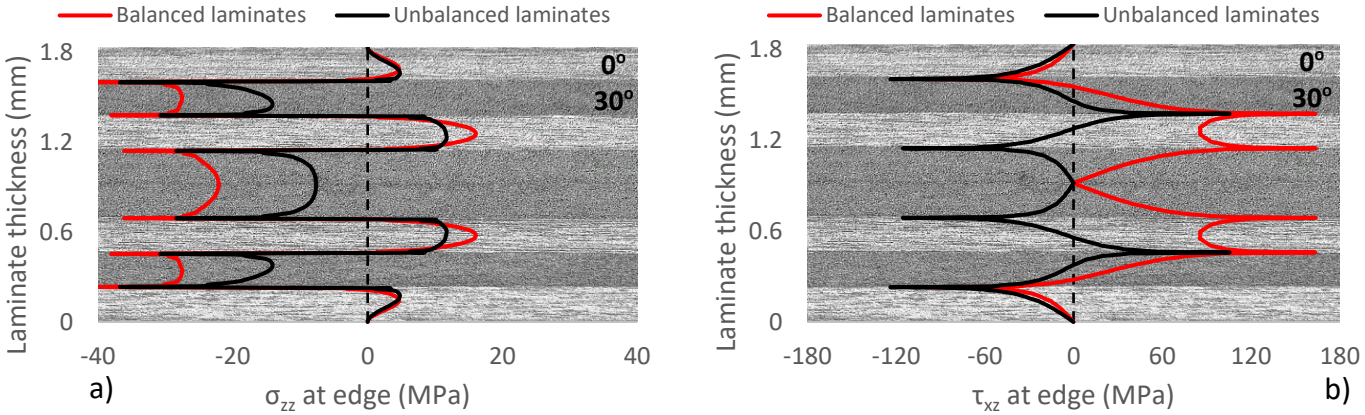

Figure 10

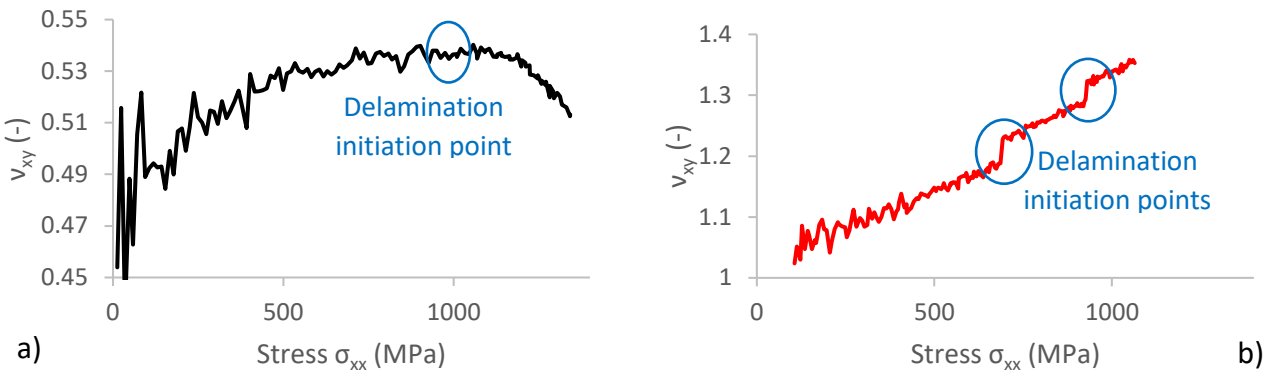

Figure 11

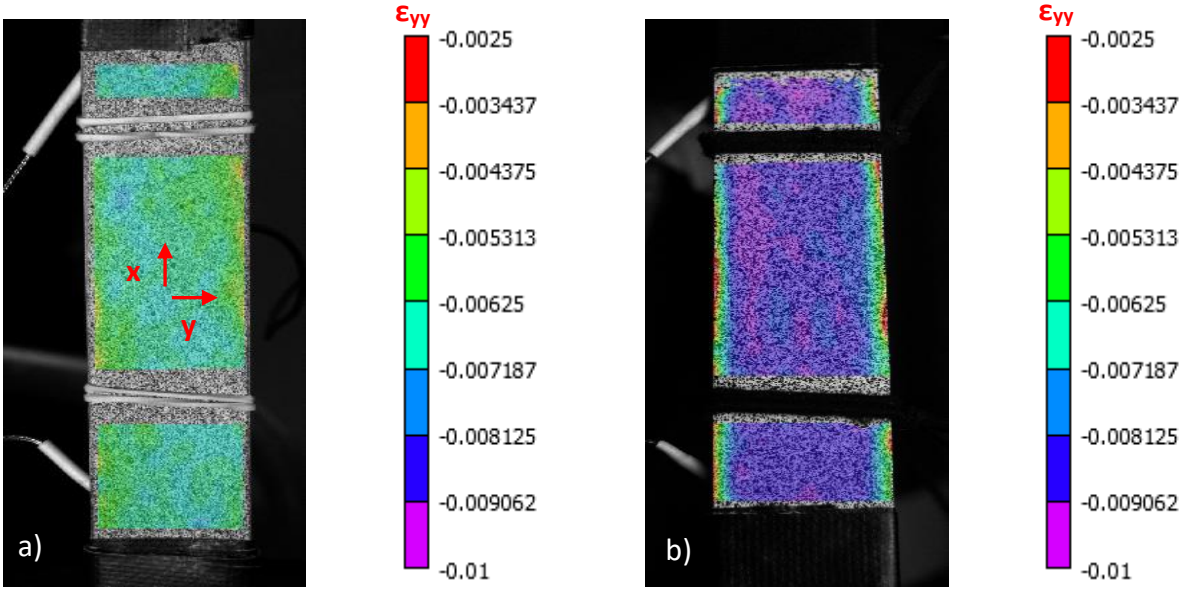

Figure 12

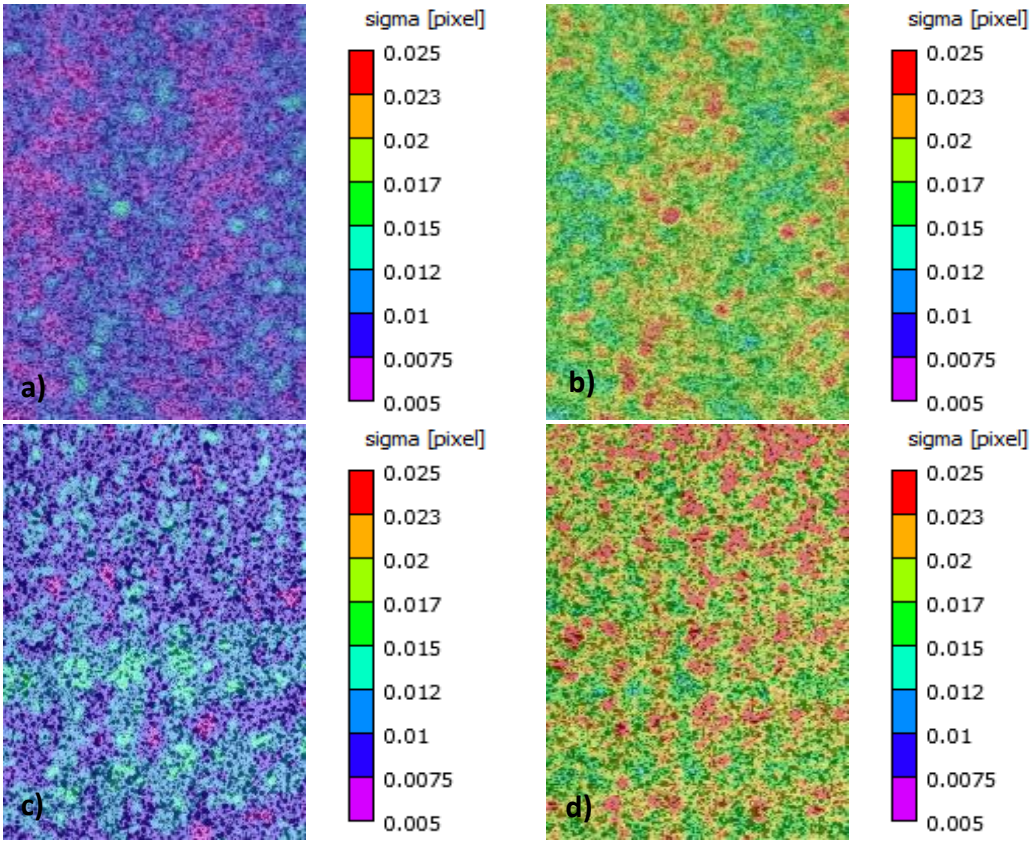

Figure 13

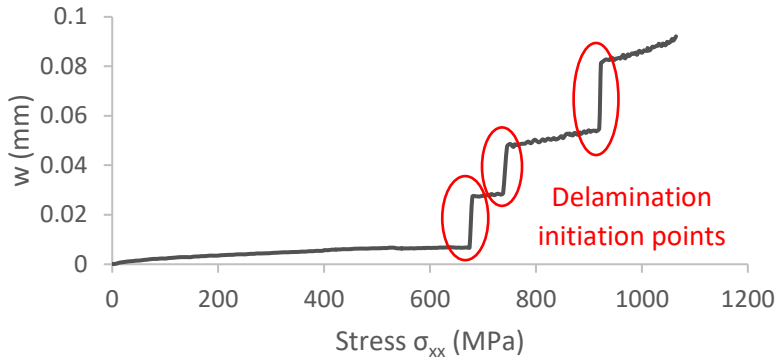

Figure 14

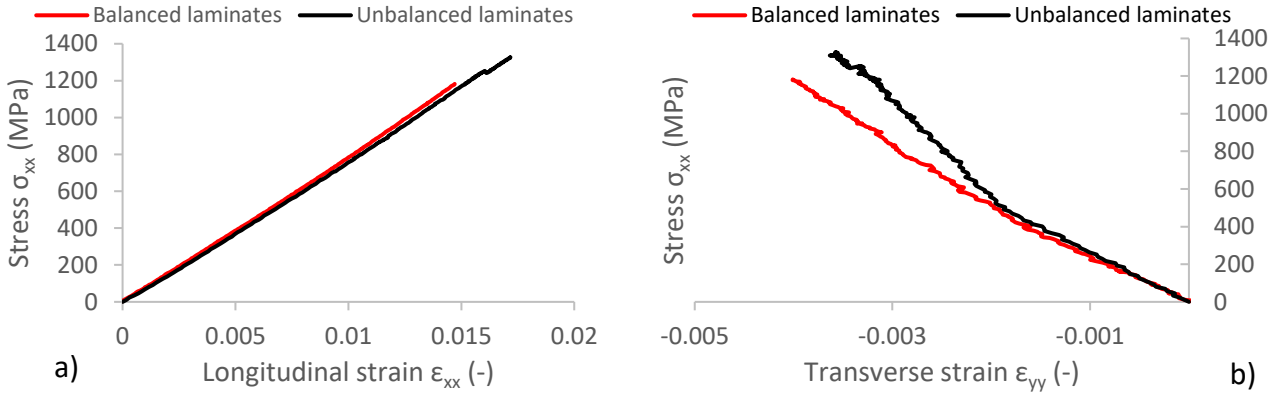

Figure 15

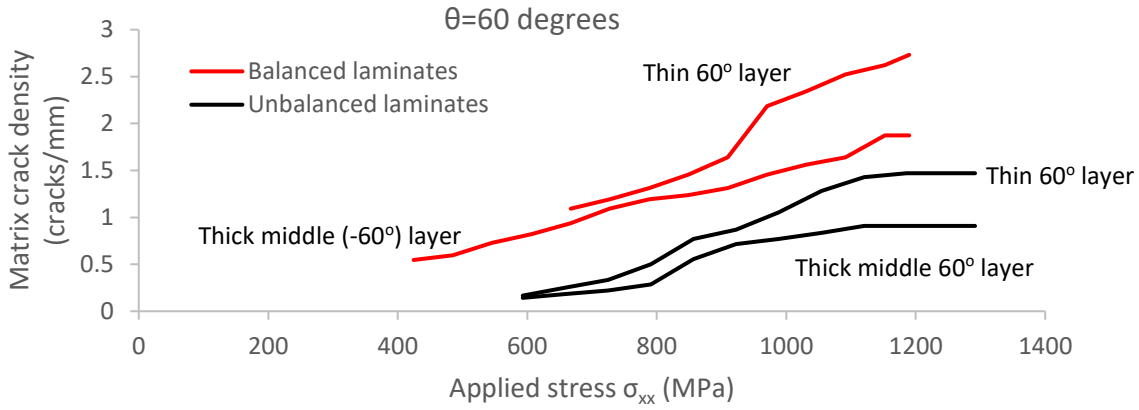

Figure 16

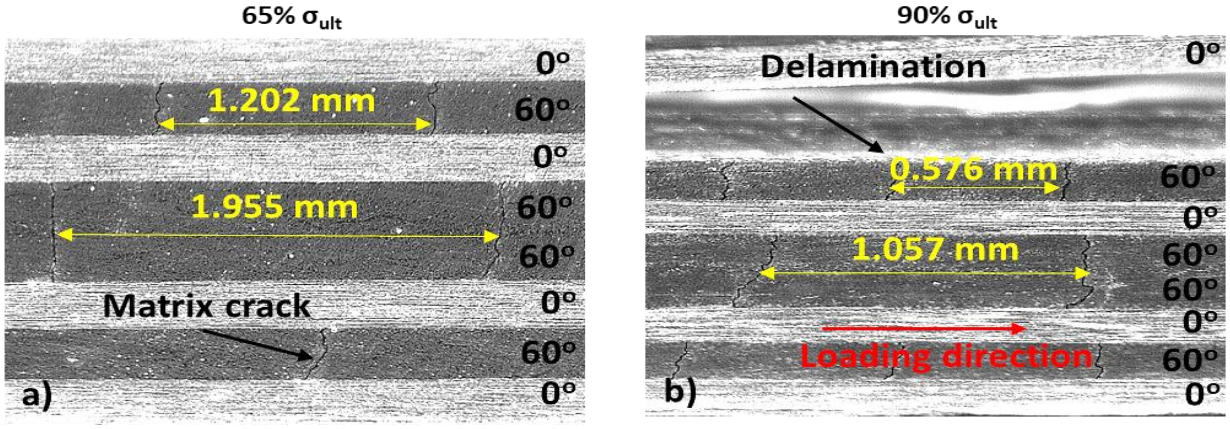

Figure 17

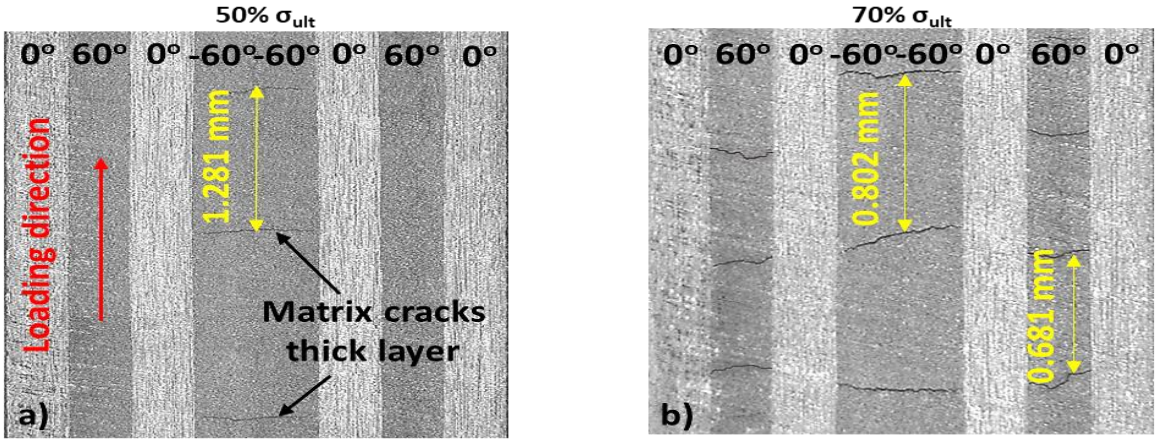

Figure 18

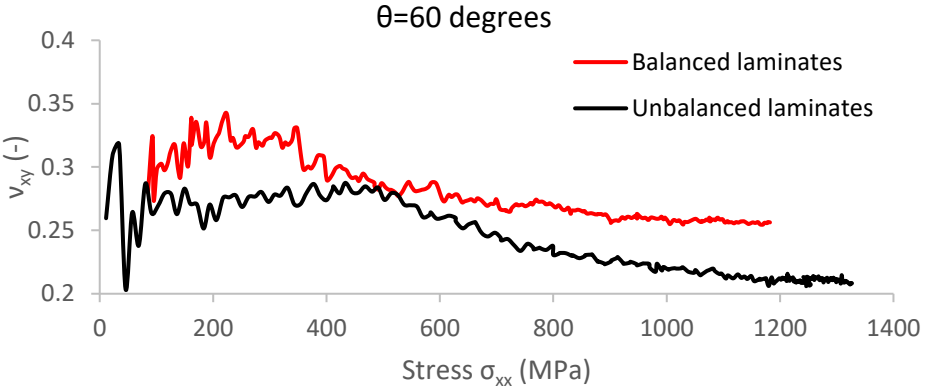

Figure 19

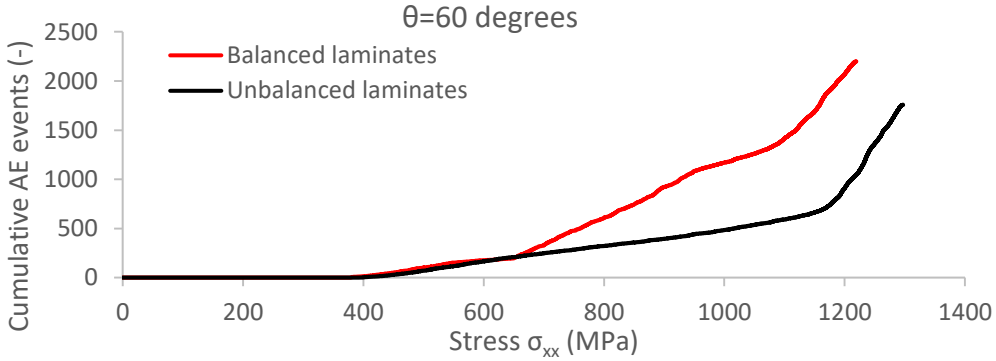

Figure 20

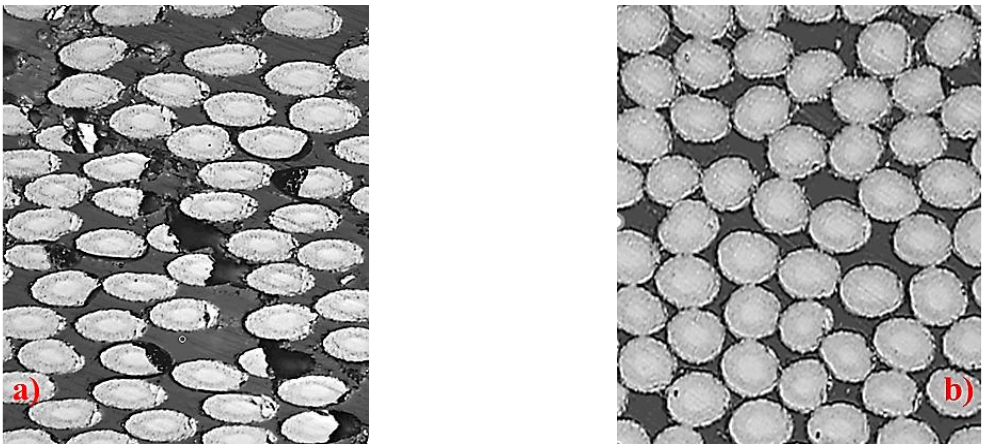

Figure 21

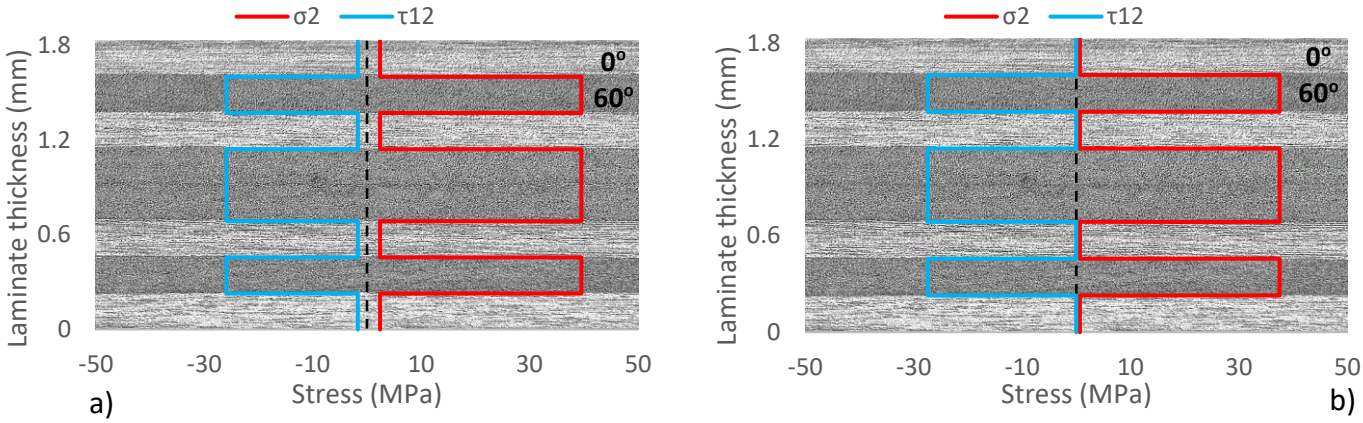

Figure 22

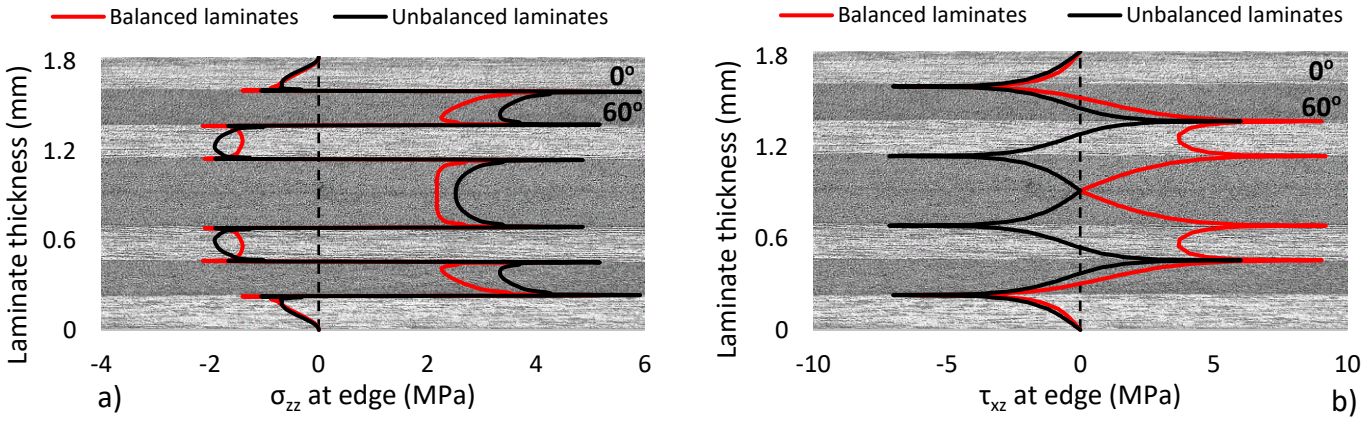

Figure 23

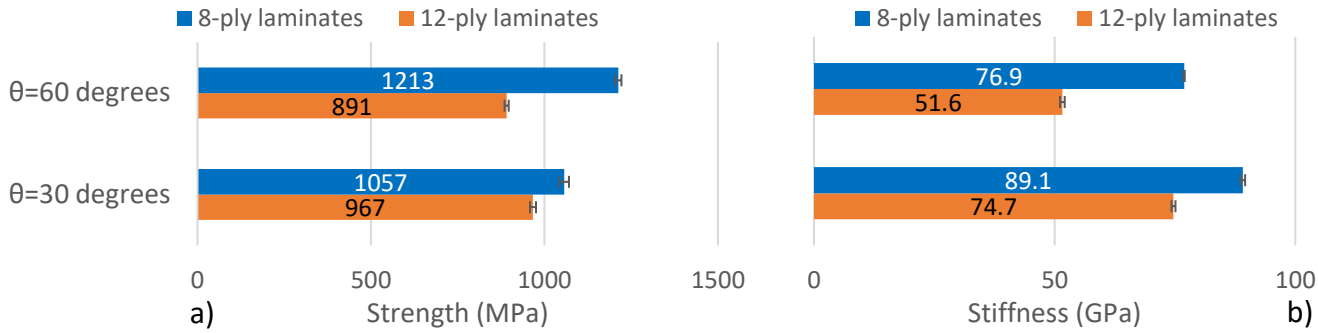

Figure 24

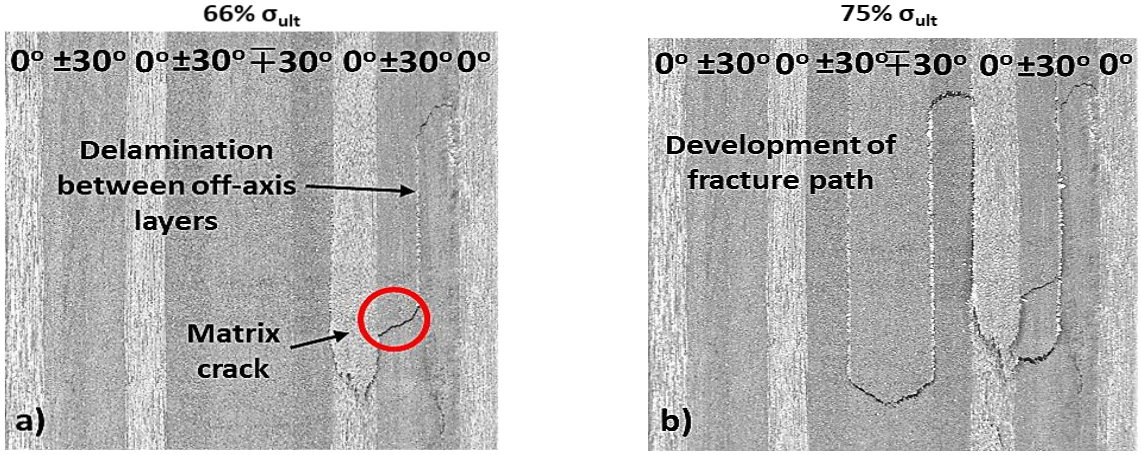

Figure 25

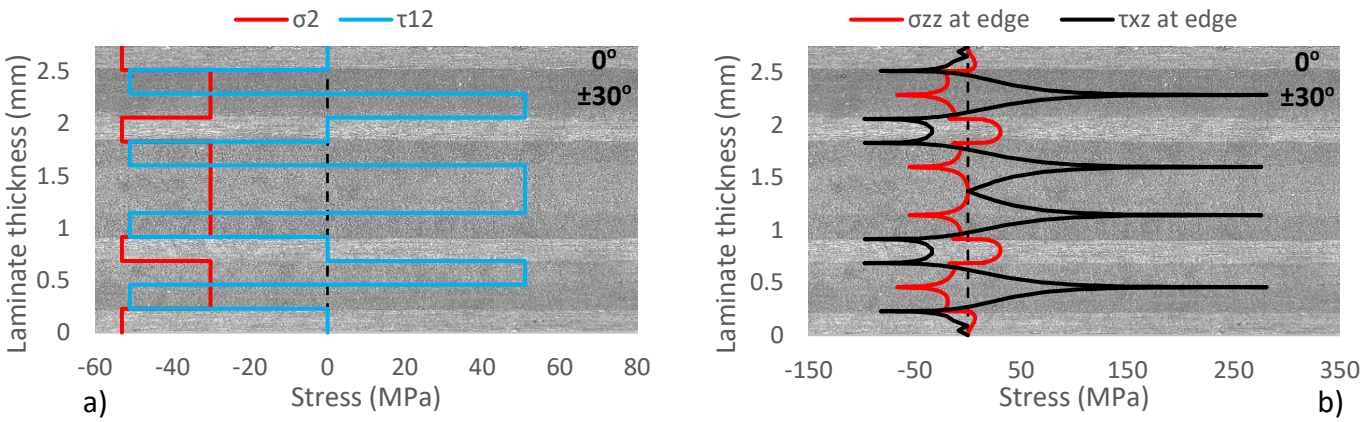

Figure 26

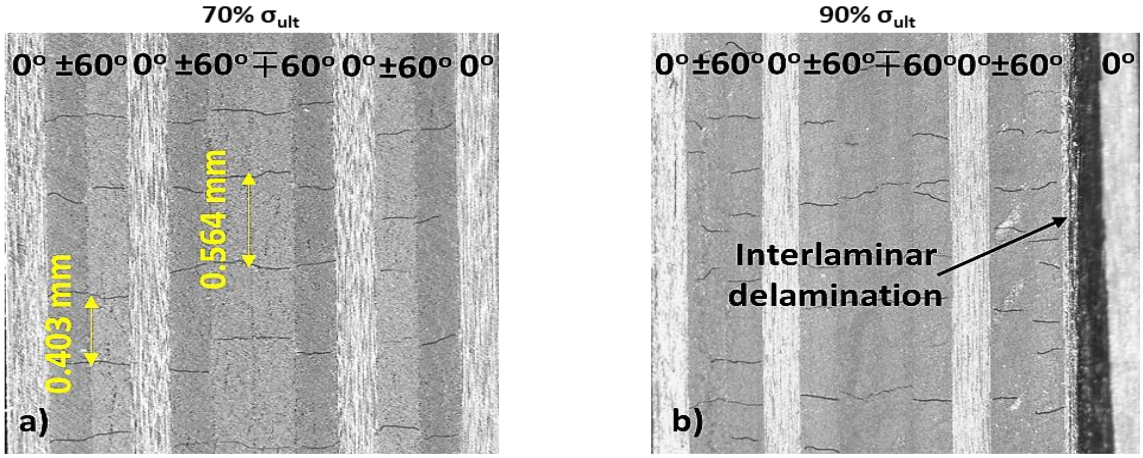

Figure 27

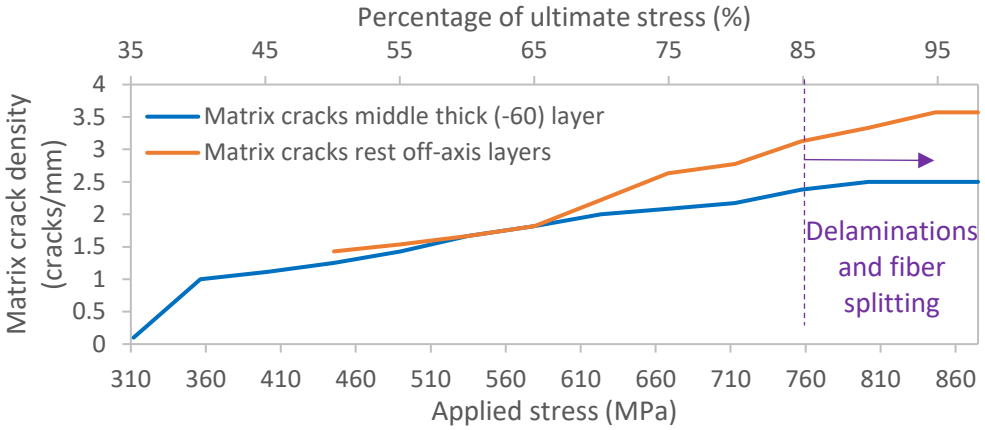

Figure 28

Figure legends

Figure 1: Experimental set-up (in-situ microscopy and DIC system).

Figure 2: Absolute biaxiality ratios λ in the off-axis layers of a) $[0^o/\theta]_{2s}$ and b) $[0^o/\theta/0^o/-\theta]_s$ laminates versus θ.

Figure 3: Experimental and linear stress-strain curves of $[0^o/30^o]_{2s}$ laminates.

Figure 4: Damage state of $[0^o/30^o]_{2s}$ laminates at stress equal to a) 80% and b) 87% of σ_{ult}.

Tables

Table 1: Material properties of the carbon/epoxy composite.

Mechanical property	***Units***	***Value***
$\sigma_{1,ult}$	MPa	2270±90
$\sigma_{2,ult}$	MPa	52.5±2
$\tau_{12,ult}$	MPa	52.3±1
E_1	GPa	130±4
E_2	GPa	9.4±0.3
G_{12}	GPa	4.1±0.1
ν_{12}	-	0.34±0.01

Table 2: DIC system configuration.

Parameter	***Units***	***Value***
Lenses	mm	23
Subset size	pixels	21
Step size	pixels	7
Resolution (x*y)	pixels	2085*896
Pixel resolution (x/y)	µm/µm	28/28
Subset resolution (x/y)	µm/µm	588/588
Sensitivity	mm/pixel	0.028
Strain sensitivity	µstrain	50
Average speckle diameter	µm	100